Environmental Science & Technology

pubs.acs.org/est

Article

Multistage Surface-Heated Vacuum Membrane Distillation Process Enables High Water Recovery and Excellent Heat Utilization: A Modeling Study

Yiming Liu, Jingbo Wang, Eric M.V. Hoek, Federico Municchi, Nils Tilton, Tzahi Y. Cath, Craig S. Turchi, Michael B. Heeley, and David Jassby*

Cite This: *Environ. Sci. Technol.* 2023, 57, 643−654

Read Online

ACCESS | Metrics & More | Article Recommendations | Supporting Information

ABSTRACT: Surface-heated membrane distillation (MD) enhances the energy efficiency of desalination by mitigating temperature polarization (TP). However, systematic investigations of larger scale, multistage, surface-heated MD system with high water recovery and heat recycling are limited. Here, we explore the design and performance of a multistage surface-heated vacuum MD (SHVMD) with heat recovery through a comprehensive finite difference model. In this process, the latent heat of condensation is recovered through an internal heat exchanger (HX) using the retentate from one stage as the condensing fluid for the next stage and an external HX using the feed as the condensing fluid. Model results show that surface heating enhances the performance compared to conventional vacuum MD (VMD). Specifically, in a six-stage SHVMD process, 54.44% water recovery and a gained output ratio (GOR) of 3.28 are achieved with a surface heat density of 2000 W m^{-2}, whereas a similar six-stage VMD process only reaches 18.19% water recovery and a GOR of 2.15. Mass and energy balances suggest that by mitigating TP, surface heating increases the latent heat trapped in vapor. The internal and external HXs capture and reuse the additional heat, which enhances the GOR values. We show for SHVMD that the hybrid internal/external heat recovery design can have GOR value 1.44 times higher than that of systems with only internal or external heat recovery. Furthermore, by only increasing six stages to eight stages, a GOR value as high as 4.35 is achieved. The results further show that surface heating can reduce the energy consumption of MD for brine concentration. The multistage SHVMD technology exhibits a promising potential for the management of brine from industrial plants.

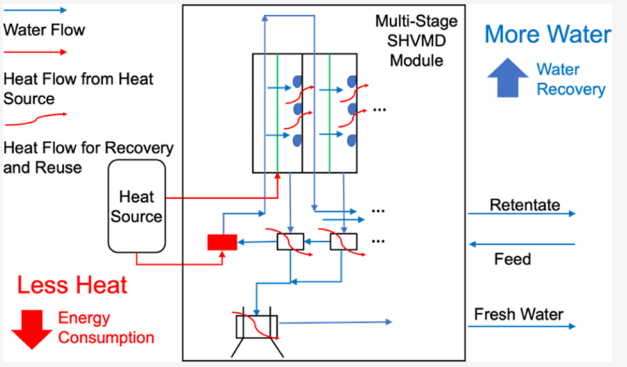

KEYWORDS: *membrane distillation, brine, surface heating, multistage, water recovery, gained output ratio*

1. INTRODUCTION

Brine is a common waste of concern from multiple industries, such as oil and gas production,[1] metal refining,[2] water desalination,[3] and food processing.[4] A common definition of a brine is an aqueous stream with total dissolved solid (TDS) concentration higher than 50,000 ppm, but in some cases, it is denoted as TDS above 70,000 ppm.[5] Specifically, some examples include brines with 100,000 ppm Na_2SO_4 that were produced during metal refining, for example, when a base was used to neutralize the strong acids used for leaching of ores;[2,6] also, a solution containing NaCl and $CaCl_2$, with total TDS as high as 89,800 ppm, was used in the processing of cucumber for pickling.[4] Instead of being directly transported to distant disposal sites,[7] high-TDS brines can be pretreated and desalinated[8] for beneficial reuse. For instance, the treated brine can be reused for fracking at an inland oil and gas extraction facility.[9] From a brine concentration or "minimal liquid discharge (MLD)" perspective, the brine volume and disposal cost are minimized. When zero liquid discharge (ZLD) is the goal, the concentrated brine is required to exceed 250,000 ppm TDS[10,11] before being fed into a thermal crystallizer.[12,13]

Membrane distillation (MD) is capable of converting high-TDS brines into distillate quality product water in a single pass,[14−16] and MD can desalinate waters of higher TDS than reverse osmosis (currently limited to ∼100,000 ppm TDS); MD also may offer a lower capital cost (particularly in applications <500 m^3 day^{-1}) than the traditional thermal distillation process.[10,17−19] However, dramatic evaporative heat

Received: September 29, 2022
Revised: December 15, 2022
Accepted: December 16, 2022
Published: December 29, 2022



ACS Publications

© 2022 American Chemical Society

Downloaded from pubs.acs.org/esthag/article-pdf/57/1/643/2704146/es2c07094.pdf by DOKUZ EYLUL UNIV user on 30 August 2026

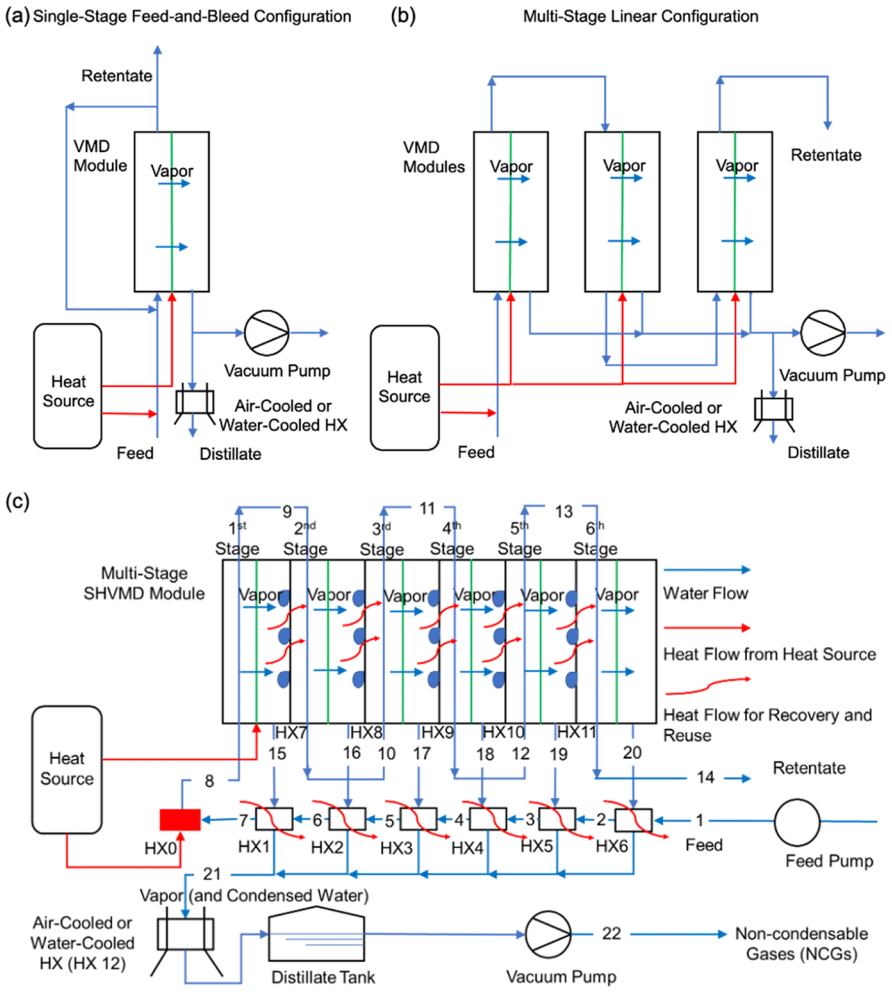

Figure 1. Flow schematics of (a) single-stage looping configuration and (b) multistage linear configuration as potential choices for high water recovery MD process. (c) Six-stage SHVMD module coupled with internal and external HXs. Inside the multistage VMD module, the green lines represent the MD membrane, whereas the black lines represent the heat-conducting wall separating each stage.

losses in the feed stream lead to a hard limit on the degree of water recovery in a single pass.[20] To target higher water recoveries, the feed stream needs to be repeatedly reheated with different process schemes used to achieve this (e.g., multistage MD, single-stage feed-and-bleed MD).[18,21−25] Interestingly, the retentate from the high-recovery MD process can be leveraged for use in salinity gradient power generation devices, which have been shown to be more effective with high-TDS streams.[26,27]

Due to the large latent heat of evaporation (2168.4−2330.9 kJ kg^{-1} at a TDS of 50,000 ppm from 90 to 20 °C),[28] thermal desalination processes are inherently energy-intensive. Therefore, heat recovery and reuse are critical to minimize energy consumption and enhance the commercial potential of thermal desalination processes. Among the various MD configurations, vacuum MD (VMD) shows higher flux and energy efficiency at the lab scale.[29,30] In VMD, a vacuum pump can create a permeate side pressure close to 0, which maximizes the driving force and flux.[31] In terms of energy efficiency, an analysis of cost-optimal solar MD showed that VMD outperformed the other configurations of MD in terms of energy consumption.[30] Furthermore, VMD has been commercially scaled up for brine desalination with many modeling[18,32−35] and experimental[35−38] studies evaluating key performance metrics. During the high-recovery VMD process, heat exchangers (HXs) are placed at different locations of the hydraulic system to recover the latent heat of evaporation. For example, the relatively cool retentate from one stage can be used as the condensing fluid to condense and recover the latent heat from the permeate stream, as shown in commercially deployed Memsys systems.[37] In addition, the cold influent feed can be used as the condensing fluid, which heats up the incoming feed stream, as shown in a multistage VMD simulation.[18]

Surface heating has been demonstrated to minimize temperature polarization (TP) by heating up the membrane−feed interface, which enables higher water recoveries and energy efficiency during brine desalination.[10,31,39−45] The heat can be delivered to the membrane surface through different mechanisms. For example, resistively heating the surface of electrically conducting membranes was achieved by applying direct or alternating currents at sufficiently high frequencies that minimize CNT oxidation.[39−43] However, the energy demand of Joule heating is high in a single-pass scenario with no heat recovery (e.g., about 4495 kJ kg^{-1} reported by Dudchenko et al.[39]) for two reasons. One reason is that some of the heat is lost to the bulk water. The second reason is that the method relies on converting electrical energy (a higher form of energy) to heat, which always incurs efficiency losses. Another example of surface heating is the integration of thermal carriers (e.g., metal mesh/shim) into the

https://doi.org/10.1021/acs.est.2c07094
Environ. Sci. Technol. 2023, 57, 643−654

Downloaded from pubs.acs.org/esthag/article-pdf/57/1/643/2704146/es2c07094.pdf by DOKUZ EYLUL UNIV user on 30 August 2026

membrane and/or flow channel that conduct externally provided heat into the membrane module.[10,31,44,45] In contrast to Joule heating, conducting heat from an external source does not require the conversion of electrical energy into thermal energy, which can lead to higher efficiency.

By carefully designing heat recovery from the evolved vapor, the advantages of surface-heated VMD (SHVMD) in a larger scale system can be exploited. Specifically, multistage membrane systems allow for effective heat recovery and recycling, which can reduce the energy needed to generate a volume of desalinated water [quantified by the gained output ratio (GOR) value]. In addition, surface heating has been demonstrated to improve the energy efficiency and water recovery during MD processes. However, we are not aware of any systematic investigations of how heat recovery can be achieved in the context of an SHVMD system. In this study, we develop a physics-based process model that enables a systematic performance analysis of a multistage SHVMD process that incorporates latent heat recovery and reuse. We demonstrate that surface heating can enhance both water recovery and process energy efficiency of SHVMD and analyze the heat and mass transfer mechanisms of both SHVMD and conventional VMD based on a simplified framework. In addition, the role of each type of HX in improving the water recovery and GOR is elucidated by comparing the process performance of different heat recovery designs in a staged SHVMD system. We further explore the system energy performance during the desalination of different brines having a range of TDS levels. Finally, the implications of multistage SHVMD system with respect to other state-of-the-art thermal desalination technologies are discussed.

2. MODEL DEVELOPMENT

2.1. System Configurations for Large-scale SHVMD Processes. Two possible configurations for the SHVMD process were explored, with the goal of achieving high water recovery and GOR. The first (and simpler) configuration is a single-stage design where part of the retentate is recycled back to the membrane inlet (i.e., feed-and-bleed configuration) (Figure 1a).[21−23] In the second configuration, a multistage system was explored, where the retentate from one stage is used as the feed to the next (Figure 1b).[18,24,25,46] In both configurations, the bulk influent feed stream is preheated, and the feed stream is additionally heated at the membrane−feed interface by the membrane surface (e.g., Joule heating, etc.). Bulk heating provides the primary thermal driving force, while surface heating is applied to mitigate TP. Condensation heat from the vapor is captured by an external air- or water-cooled HX.

The capital expense (CapEx) of thermal desalination systems is relatively small compared to the operating expense (OpEx).[47,48] HXs and membranes are the two primary components of the CapEx. They are evaluated through two metrics, membrane surface area per liter of produced distilled water and HX surface area per liter of produced distilled water.[26,27] In terms of OpEx, the cost of heat dominates.[47] Therefore, all commercially used thermal desalination units rely heavily on heat recovery and reuse in an effort to minimize the injection of new heat into the system,[17] which is also true for MD systems.[17] In practice, this translates into using multistage, rather than single-stage, systems, which enable heat recovery and reuse.[18] GOR and energy efficiency (defined as the ratio between the free energy of separation of the produced solutions and the consumed heat) are used as the parameters to evaluate the energy performance of the system.[26,27]

HXs are widely used in MD processes to capture and recycle heat (both sensible and latent heat). For example, air gap MD achieves the recovery of the latent heat of condensation from the vapor by inserting a cool surface into the module where the vapor is condensed and the heat is captured and recycled by a cool saline stream.[49−51] Previous studies on multistage VMD explored placing HXs in the permeate stream and using the retentate from one stage as the condensing fluid, which is then heated and reused as feed in the next stage,[25,37,38,52] using the feed stream as the condensing fluid, which heats up as the entire feed stream for the process,[18] or both.[36] Based on these studies, the heat recovery design of the SHVMD process explores both types of heat recovery designs.

2.2. Multistage SHVMD System Overview. A six-stage model was constructed and used as a test case of the SHVMD process (Figure 1c). The simulated system contains both external HXs (i.e., HXs 1 through 6 that use the original feed as the condensing fluid) and internal HXs (i.e., HXs 7 through 11 that use retentate as the condensing fluid, which is then reused as feed in the next stage) that capture and recycle heat. Prior to entering the MD module, the cold influent feed stream (stream 1) is preheated by the uncondensed vapor (HXs 1−6) from all the six stages of the MD module and an external heat source (HX 0), resulting in a preheated feed stream (stream 8) that enters the first stage. In the first stage, the heated water (stream 8) is vaporized along the membrane surface and passes across the membrane into the permeate stream that is under vacuum; the membrane retentate (stream 9) flows to the next stage. In the permeate stream (stream 15), the vapor is condensed on an internal HX (HX 7), with the retentate (stream 9) from the previous stage serving as the condensing fluid. This process is repeated as the retentate from each stage passes to the next (HXs 7−11). To better explain this process, stream 9 is used as an example. At the inlet of stage 2, the vapor at the outlet of stage 1 does not condense on stream 9 because the vapor and condensing fluid have the same temperature. However, after entering the inlet, the temperature of stream 9 starts dropping along the module length due to evaporation. When the temperature drops below the vapor temperature at the corresponding location, the vapor generated from stream 8 starts condensing on stream 9, which raises the fluid temperature. Therefore, the temperature of stream 9 is a balance between the first stage vapor condensation and the second stage water evaporation. Any uncondensed vapor not recovered on the internal HX is passed along to the external HX (HXs 1−6) for further condensation; any residual vapor not condensed on the internal or external HXs is captured using an air-cooled or water-cooled condenser. Critically, heat can be added to the membrane−water interface at any stage within the process, which raises the local water temperature and reverses TP.

2.3. Mass and Energy Balance of the Multistage SHVMD Process. A black box model is used to show the mass and energy conservation in the boundaries of the six-stage SHVMD process (Figure 2). The mass balance can be expressed by

$$\dot{m}_0 = \dot{m}_6 + \dot{m}_v \quad (1)$$

where $\dot{m}_0$, $\dot{m}_6$, and $\dot{m}_v$ (kg s^{-1}) are the mass flow rates of the influent feed (stream 1), the retentate from the sixth stage (stream 14), and the vapor (including the condensed vapor)

Downloaded from pubs.acs.org/esthag/article-pdf/57/1/643/2704146/es2c07094.pdf by DOKUZ EYLUL UNIV user on 30 August 2026

https://doi.org/10.1021/acs.est.2c07094
Environ. Sci. Technol. 2023, 57, 643−654

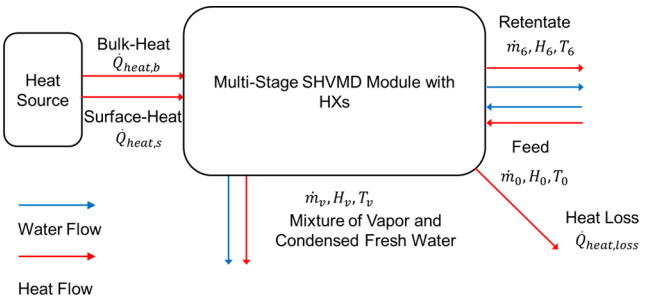

Figure 2. Black box model for mass and energy conservation in the six-stage SHVMD system.

(stream 21), respectively. The energy balance is described by the conservation of enthalpy, which can be determined by

$$\dot{m}_0 H_0 + \dot{Q}_{\text{heat,b}} + \dot{Q}_{\text{heat,s}} = \dot{m}_6 H_6 + \dot{m}_v H_v + \dot{Q}_{\text{heat,loss}} \tag{2}$$

where $\dot{Q}_{\text{heat,b}}$, $\dot{Q}_{\text{heat,s}}$, and $\dot{Q}_{\text{heat,loss}}$ (W) are the heat added to the bulk feed, heat added to the membrane surface, and heat lost during distillation and heat exchange, respectively, and H_0, H_6, and H_v (J kg^{-1}) are the average specific enthalpies along the module length of the influent feed, the final retentate, and the vapor (including condensed water), respectively. Heat loss is quantified by accounting for a percentage of ambient heat loss (5.5%) during each heat transfer step inside this system (see Section S1 for details). Because stream 21 is a mixture of vapor and condensed water, its specific enthalpy can be written as

$$H_v = H_v' + [1 - (\alpha_{in} + \alpha_{ex})]\Delta H_c \tag{3}$$

where α_{in} and α_{ex} are the portions of the vapor that condenses on the internal HX and on the external HX, respectively, H_v' (J kg^{-1}) is the average specific enthalpy along the module length of condensed water, and ΔH_c ($=H_v' - H_v$) (J kg^{-1}) is the average latent heat of condensation along the module length of the distillate. Substituting eqs 3 into 2, the final form of the energy balance is

$$\dot{Q}_{\text{heat,b}} + \dot{Q}_{\text{heat,s}} + \alpha_{in}\dot{m}_v\Delta H_c + \alpha_{ex}\dot{m}_v\Delta H_c = \dot{m}_6(H_6 - H_0) + \dot{m}_v(H_v' - H_0) + \dot{m}_v\Delta H_c + \dot{Q}_{\text{heat,loss}} \tag{4}$$

where on the left-hand side of eq 4, $\alpha_{in}\dot{m}_v\Delta H_{vap}$ (W) is the internally recovered heat, and $\alpha_{ex}\dot{m}_v\Delta H_{vap}$ (W) is the externally recovered heat. On the right-hand side of eq 4, $\dot{m}_6(H_6 - H_0)$ is the difference in enthalpy as sensible heat between the final retentate (stream 14) and the cold influent feed (stream 1), $\dot{m}_v(H_v' - H_0)$ (W) is the difference in enthalpy as sensible heat between the final vapor (stream 21) and the cold influent feed (stream 1), and $\dot{m}_v\Delta H_{vap}$ (W) is the latent heat required to produce the vapor.

2.4. Heat and Mass Transfer in the Multistage SHVMD Process. We developed a comprehensive finite difference process model that captures the temperature, salinity, water and heat flux, and the overall water recovery and energy efficiency of a full-scale multistage SHVMD system. Previously, we demonstrated a single-stage direct-heated VMD (DHVMD) model and validated the model against experimental data using real wastewater and synthetic solutions.[10] Here, we extend this single-stage model to our current multistage design. Detailed assumptions and parameters of the model are shown in Section S1 of the Supporting Information.

For each stage of the SHVMD process, the heat transfer and mass transfer are divided into two parts, one inside the feed channel and the other outside the feed channel. Each part of the heat transfer and mass transfer is described by their own governing equations. The heat and mass transfer mechanisms in a multistage system are different from a single-stage system, as the heat of condensation, obtained from the condensation of vapor, is captured and reused in the next stage (and in the feed stream). Modified governing equations for heat and mass transfer inside a single stage of a multistage system are shown in Section S2 of the Supporting Information.

The latent heat of condensation trapped within the water vapor generated during the MD process can be recovered internally (when the vapor is condensed using the retentate from the previous stage) or externally (if the vapor is condensed on the incoming feed stream and on the air-cooled or water-cooled HX) (Figure 3). In both cases, heat recovery is

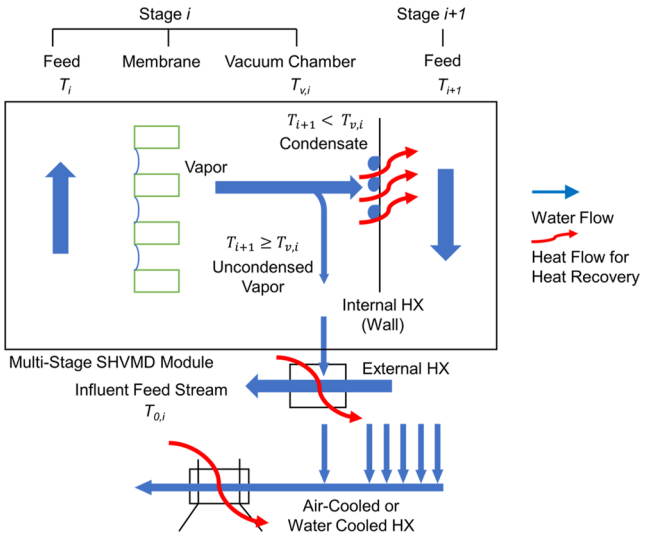

Figure 3. Schematic illustration of the interstage (between stage i and stage $i + 1$) heat and mass transfer mechanisms in the multistage SHVMD process. Inside the vacuum line, the vapor can either condense on the internal HX or condense on the external HX.

constrained by the reduced saturation temperature of vapor, which is a function of the depth of the applied vacuum (Figure S1). The derivation of the governing equations for heat and mass transfer is based on other multistage VMD and vacuum multi-effect MD (V-MEMD) formulations[18,32−35]

$$\dot{m}_v\Delta H_c = \sum_{i=1}^{N-1}\dot{Q}_{\text{heat, in},i} + \sum_{i=1}^{N}\dot{Q}_{\text{heat, ex},i} + \dot{Q}_{\text{heat,ac}} + \sum_{i=1}^{N-1}\dot{Q}_{\text{heat,loss, in},i} + \sum_{i=1}^{N}\dot{Q}_{\text{heat, loss,ex},i} + \dot{Q}_{\text{heat,loss,ac}} \tag{5}$$

where $\dot{Q}_{\text{heat,in},i}$ (W) is the heat recovered by the internal HX between stage i and stage $i + 1$ (i = 1−5, HXs 7−11), $\dot{Q}_{\text{heat,ex},i}$ (W) is the heat recovered at the external HX in stage i (i = 1−6, HXs 1−6), $\dot{Q}_{\text{heat,ac}}$ is the heat recovered at the air-cooled or water-cooled HX (HX 12), and $\dot{Q}_{\text{heat,loss,in},i}$ (W), $\dot{Q}_{\text{heat,loss,ex},i}$ (W), and $\dot{Q}_{\text{heat,loss,ac}}$ (W) are the heat losses associated with $\dot{Q}_{\text{heat,in},i}$, $\dot{Q}_{\text{heat,ex},i}$, and $\dot{Q}_{\text{heat,ac}}$, respectively. The following symbols also have a lowercase i to denote the stage i ($1 \leq i$

Downloaded from pubs.acs.org/esthag/article-pdf/57/1/643/2704146/es2c07094.pdf by DOKUZ EYLUL UNIV user on 30 August 2026

https://doi.org/10.1021/acs.est.2c07094
Environ. Sci. Technol. 2023, 57, 643−654

$\leq N$, $N = 6$). Vapor condensed on the internal HX passes its heat to the feed stream in the subsequent stage. Importantly, the vapor will condense only if the vapor temperature (considered the same as the feed temperature) is greater than the next-stage feed temperature, and the next-stage feed temperature is lower than the reduced saturation temperature at the applied vacuum level. The internal heat transfer can be expressed as

$$\text{Ø}_{\text{in},i,x} = \begin{cases} \text{Ø}_{\Delta H_c,i,x} - \text{Ø}_{\text{loss,in},i,x} \ (\text{if } T_{i+1,r,x} \\ \quad < T_{\text{v},i} \text{ and } 1 \\ \quad \leq i \\ \quad < 6) \\ 0 \ (\text{if } T_{i+1,r,x} \geq T_{\text{v},i} \text{ or } i = 6) \end{cases} \tag{6}$$

where $\text{Ø}_{\text{in},i,x}$ (W m^{-2}) represents the local interstage heat flux along the channel length, $\text{Ø}_{\Delta H_c,i,x}$ (W m^{-2}) represents the local flux of latent heat of condensation along the channel length between stage i and stage $i + 1$, and $\text{Ø}_{\text{loss,in},i,x}$ (W m^{-2}) represents the flux of heat lost during the interstage heat exchange between stage i and stage $i + 1$; $T_{i+1,r,x}$ is the bulk feed temperature in stage $i + 1$, and $T_{\text{v},i}$ is the vapor temperature in stage i. The lowercase x ($0 \leq x \leq L$, L is the length of the flow channel) in the symbols represents a specific location. In addition, the reverse-flow direction of one stage against the adjacent stage is represented by a lowercase r in the symbols. Vapor that does not condense on the internal HX then moves to the external HX where it can condense on the influent feed stream. As before, the influent feed temperature cannot exceed the saturation temperature of the vapor. The maximum heat-exchanging capacity of the external HX ($\dot{Q}_{\text{heat,ex},i,\text{max}}$, W) is determined by

$$\dot{Q}_{\text{heat, ex},i,\text{ max}} = \begin{cases} \rho_{0,i} Q_{0,i} \int_{T_{0,i+1}}^{T_{\text{v},i}} c_{\text{p},0,i} \text{d}T \ (\text{if } 1 \leq i < 6) \\ \rho_{0,i} Q_{0,i} \int_{T_0}^{T_{\text{v},i}} c_{\text{p},0,i} \text{d}T \ (\text{if } i = 6) \end{cases} \tag{7}$$

where $\rho_{0,i}$ (kg m^{-3}), $Q_{0,i}$ (m^3 s^{-1}), $c_{\text{p},0,i}$ (J kg^{-1} K^{-1}), and $T_{0,i}$ (K) are the density, volumetric flow rate, specific heat capacity, and temperature of the influent feed stream entering HX i (stream $7 - i$). The amount of heat that is effectively transferred to the feed stream is limited by the heat-exchanging capacity of the external HX. Therefore, the external heat transfer can be calculated as

$$\dot{Q}_{\text{heat, ex},i} = \begin{cases} \int_0^L (\text{Ø}_{\Delta H_c,i,x} - \text{Ø}_{\text{in},i,x} - \text{Ø}_{\text{loss,ex},i,x}) W \text{d}x \\ \quad (\text{if } \dot{Q}_{\text{heat},\Delta H_c,i} - \dot{Q}_{\text{heat, in},i} \\ \quad < \dot{Q}_{\text{heat, ex},i,\text{max}}) \\ \dot{Q}_{\text{heat, ex},i,\text{ max}} \ (\text{if } \dot{Q}_{\text{heat},\Delta H_c,i} - \dot{Q}_{\text{heat, in},i} \\ \quad \geq \dot{Q}_{\text{heat, ex},i,\text{max}}) \end{cases} \tag{8}$$

where W (m) is the width of the flow channel, $\text{Ø}_{\text{loss,ex},i,x}$ (W m^{-2}) represents the flux of heat lost from the external HX i, and $\dot{Q}_{\text{heat},\Delta Hc,i}$ (W) is the flow of latent heat of condensation from the produced vapor in HX i.

Overall, based on the equations above (eqs 6−8), the performance of all HXs is constrained by the reduced saturation temperature ($T_{\text{v},i}$, i = 1−6) of each stage. Other equations describing heat and mass transfer outside the feed channel are detailed in Section S2 of the Supporting Information.

2.5. Performance Metrics of the Multistage SHVMD Process. Systematic performance metrics are determined based on both energy and mass balances. Water recovery (Y) is calculated by

$$Y = \frac{W \sum_{i=1}^{i=6} \int_0^L J_{i,x} \text{d}x}{\rho_0 Q_0} \tag{9}$$

where $J_{i,x}$ (kg m^{-2} s^{-1}) is the local vapor flux along the module length in stage i, ρ_0 (kg m^{-3}) is the density of the influent feed stream (stream 1), and Q_0 (m^3 s^{-1}) is the volumetric flow rate of the influent feed stream (stream 1). In addition to water recovery, both the membrane surface area normalized by the volume of produced distilled water and the HX surface area normalized by the volume of produced distilled water are evaluated. Specific membrane surface area ($A_{\text{m,p}}$, in m^2 s L^{-1}) is determined by

$$A_{\text{m,p}} = \frac{A_{\text{m}}}{Q_{\text{p}}} \tag{10}$$

where A_{m} (m^2) is the total membrane surface area, and Q_{p} (L s^{-1}) is the total flow rate of the permeate. The specific HX surface area ($A_{\text{HX,p}}$, in m^2 s L^{-1}) is calculated by

$$A_{\text{HX,p}} = \frac{A_{\text{HX}}}{Q_{\text{p}}} \tag{11}$$

where A_{HX} (m^2) is the total HX surface area.

GOR is a typical performance metric used to gauge the energy efficiency of a thermal desalination system

$$\text{GOR} = \frac{\dot{m}_{\text{v}} \Delta H_{\text{vap}}}{\dot{Q}_{\text{heat,s}} + \dot{Q}_{\text{heat,b}}} \tag{12}$$

Intuitively, the GOR value represents "the number of times" the latent heat is reused in the system for water evaporation, with higher GOR values representing a system that consumes less energy to evaporate a given volume of water.[53] In addition to GOR, the energy efficiency (η) is calculated by

$$\eta = \frac{\dot{m}_0 W_{\text{min}}}{\dot{Q}_{\text{heat,s}} + \dot{Q}_{\text{heat,b}}} \tag{13}$$

where W_{min} (J kg^{-1}) is the minimum work of separation to produce water from the feed stream (e.g., 1.91×10^4 J kg^{-1} = 5.3 kW h m^{-3} for hypersaline brines[9]). Other supporting performance metrics, such as the fraction of condensed water from vapor (F) that characterizes the efficiency of internal heat recovery and reuse, and the amount of heat recovered by external HX and air-cooled or water-cooled condenser, are detailed in Section S3 of the Supporting Information.

3. RESULTS AND DISCUSSION

3.1. Enhanced Performance Enabled by Surface Heating. The impact of membrane surface heating density (kW m^{-2}) on a six-stage SHVMD system, in terms of water recovery and GOR, was explored (Figure 4). We select three

Downloaded from pubs.acs.org/esthag/article-pdf/57/1/643/2704146/es2c07094.pdf by DOKUZ EYLUL UNIV user on 30 August 2026

https://doi.org/10.1021/acs.est.2c07094
Environ. Sci. Technol. 2023, 57, 643−654

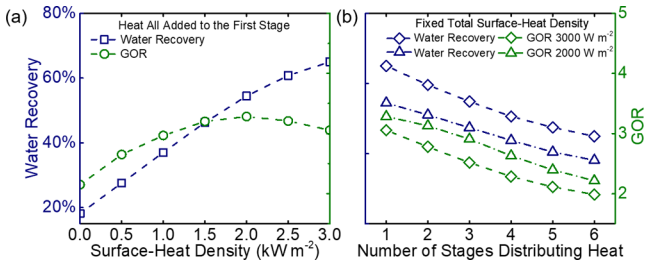

Figure 4. Water recovery and GOR of the six-stage SHVMD system as a function of (a) surface heat added to only the first stage (from 0 to 3000 W m^{-2}) and of the (b) number of stages where a fixed amount of surface heat (density in 2000 and 3000 W m^{-2}) is distributed sequentially. Both (a) and (b) share the same *y*-axes of water recovery (on the left) and GOR (on the right).

increasing surface heat densities (0, 2000, and 3000 W m^{-2}) for analysis. The maximum GOR is achieved at a heat input of 2000 W m^{-2} surface heat density. For 2000 and 3000 W m^{-2} heat densities, the total surface-added heat (across a total membrane area of 12.96 m^2) is calculated to be 25,920 and 38,880 W, respectively. Surface heating enhances the six-stage SHVMD system performance in terms of water recovery and GOR. Initially, we explored the impact of adding heat only to the first stage of the system (Figure 4a). Below 2000 W m^{-2}, both water recovery and GOR increase with the surface heat input, implying that the surface heat input effectively evaporates water and that the heat could be used more efficiently compared to bulk heating (as exemplified by the increasing GOR). However, beyond the surface heat density of 2000 W m^{-2}, a trade-off is present between GOR and water recovery, where GOR starts decreasing, whereas water recovery keeps increasing. Therefore, even though the additional heat can still be used to evaporate water, this heat is not efficiently recovered and reused. A further analysis on how GOR changes with surface heat density is presented in Section S3 of the Supporting Information. The membrane surface temperature profile in the first stage is shown as an example in Figure 5c (solid line, equal to vapor temperature). The membrane surface temperature increases with the increasing surface heat input but does not exceed the preheated feed temperature at the inlet (90 °C).

The addition of surface heat (2000 and 3000 W m^{-2} in total) to each stage (equal heat density applied to all membranes) was also evaluated (Figure 4b). Specifically, a fixed amount of surface heat (2000 and 3000 W m^{-2}) is equally spread to different number of successive stages. As the number of stages increases, both water recovery and GOR decrease (Figure 4b). The decline in GOR means that the surface heat is reused for fewer times, based on the intuitive interpretation of GOR (see Section 2.5 for details). When the surface heat is added to the feed in one stage, more vapor is produced. The internal HX captures the additional heat in the vapor and reuses the heat to heat the feed going into the next stage. The same heat capture and reuse is repeated until the final stage (stage 6). If the heat is added to stage 1, this process will repeat five times until stage 6. However, if the heat is added to later stages, there is less opportunity to capture and reuse the added heat. Thus, the surface heat added to stage 1 is reused the most, and concentrating all the surface heat in stage 1 achieves the highest GOR values. Also, the most reused heat leads to the most total heat input for water evaporation and thereby the highest water recovery.

The addition of heat to the membrane surface and to the bulk feed (through the feed channel) was also compared (Figure S3). We evaluate 100% surface heating, 50% surface

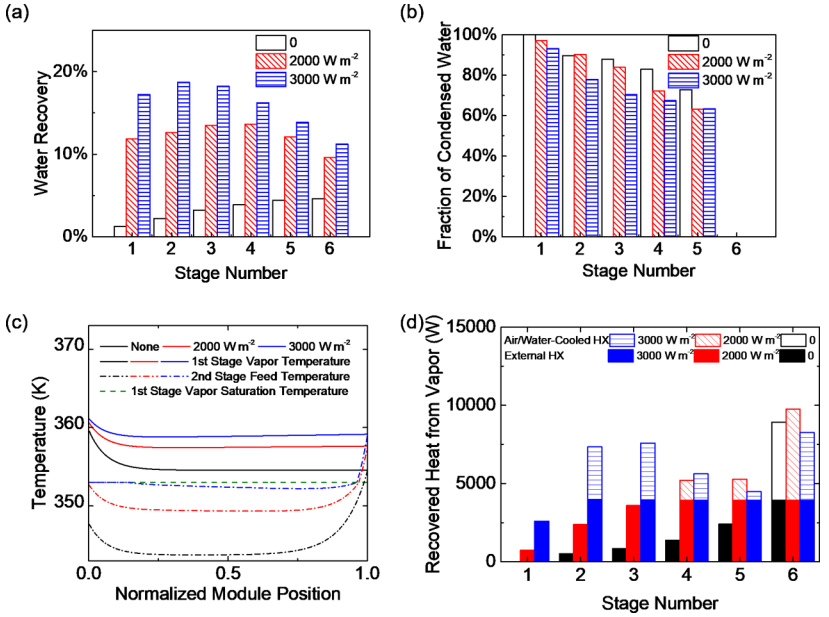

Figure 5. Performance of the six-stage SHVMD process with the density of surface heat input to the first stage of 0 (conventional VMD), 2000, and 3000 W m^{-2}. (a) Water recovery per stage and (b) fraction of condensed water out of produced vapor (vapor condensation efficiency) per internal HX inside the VMD module. (c) Vapor temperature (membrane surface temperature) and the reduced saturation temperature in the first stage and the temperature of feed in the second stage as condensing fluid as a function of normalized channel length (2.4 m long). (d) Heat recovered from the effluent vapor from each stage by the external HX (where it is recovered by the incoming feed stream) and by the air-/water-cooled HX (where it is lost to the environment). Solid bars represent the heat captured by the external HX for each stage, whereas empty and hatched bars represent the energy lost to the environment from each stage on the air-/water-cooled HX.

Downloaded from pubs.acs.org/esthag/article-pdf/57/1/643/2704146/es2c07094.pdf by DOKUZ EYLUL UNIV user on 30 August 2026

https://doi.org/10.1021/acs.est.2c07094
Environ. Sci. Technol. 2023, 57, 643−654

heating + 50% bulk heating, and 100% bulk heating conditions. Model results show that under the same heat input, surface heating demonstrates better performance in water recovery and GOR compared to bulk heating (see Section S4 for details), which are consistent with the model results in a single-pass VMD system.[10]

3.2. Mechanisms of Internal and External Heat Recovery. A stage-by-stage analysis was performed to determine the heat and mass transfer responsible for internal and external heat recovery in a multistage configuration. Note that the following analysis is focused on the absolute value of internally versus externally recovered heat instead of their relative values. The internal heat and mass transfer mechanisms were investigated by tracking two factors, water recovery for a given stage (defined in eq S28) and the fraction of vapor condensation per stage (defined in eq S29). The internally recovered heat reuse (in W) is directly related to the mass flow of condensed water (in kg s^{-1}) using latent heat of condensation (in J kg^{-1}). Furthermore, the mass flow of condensed water (in kg s^{-1}) equals the total mass flow rate of produced vapor (in kg s^{-1}) multiplied by the vapor condensation efficiency (i.e., fraction of produced vapor that is condensed into water).

To analyze the internal heat recovery, mass transfer in terms of vapor production and vapor condensation was examined. The addition of surface heat to the first stage (2000 or 3000 W m^{-2}) increases the water recovery for each stage (Figure 5a). As a result, the total vapor flow is greater with a higher surface heat input. In contrast, the vapor condensation efficiency is lower. The proportion of vapor that is condensed decreases with increased surface heat input for almost every stage (Figure 5b). Therefore, the decrease in the vapor condensation efficiency limits the total mass flow of condensed water after a certain surface heat input (2000 W m^{-2} here). As a result, the mass flow of condensed water and internally recovered heat have a smaller increase compared to the increase in surface heat input, which leads to a reduced GOR.

The temperature of vapor in one stage and feed in the next stage can be used to track the vapor production for a given stage and vapor condensation on the subsequent stage. Vapor production is governed by the temperature of the feed stream and the applied vacuum pressure, whereas internal vapor condensation is determined by the vacuum pressure and temperature difference between the vapor and feed stream in the subsequent stage. As an example of all six stages, the temperature profiles for a permeate channel (2.4 m in length) between the first and second stages under different surface heat conditions were calculated (Figure 5c). Membrane surface temperature at each point along the module length is treated as the vapor temperature at that point. As the membrane surface temperature increases, due to the surface heat input, the temperature of the water along the membrane/water interface increases, which increases the driving force for water vapor formation, the vapor flux, and the vapor temperature (Figure 5c). In the next stage (stage 2), the temperature of the feed stream is a function of the mass of vapor that is condensed (as the feed stream serves as the condensing fluid for the vapor generated in the previous stage—stage 1); as more heat is provided to the surface of the membrane in stage 1, more vapor is produced, which when condensed increases the temperature of the feed in stage 2 (Figure 5c). Also, as more heat is added to the membrane surface in stage 1, evaporative heat losses in this stage are mitigated, which increase the temperature of stage 1 retentate—the feed in stage 2. However, if the temperature of the condensing stream is higher than the vapor saturation temperature (under vacuum), then no condensation and heat recovery can take place (eq 6). Hence, adding excess heat to the membrane/water interface in stage 1 increases the water recovery from that stage but decreases the portion of surface-provided heat that can be recovered in stage 2, which can lead to reduced GOR. Overall, with surface heating, both the vapor temperature of one stage and the bulk feed temperature of the next stage increase; as a result, stage 1 produces dramatically more vapor (Figure 5a), while a smaller percent of mass of vapor can be condensed in stage 2, leading to the overall lower heat recovery between the stages (Figure 5b).

Recovering heat on the external HXs is a function of the efficiency of the internal HX, with the maximum recovery limited by the reduced saturation temperature in the condenser (a function of the applied vacuum) (eq 8). The amount of heat available for external heat recovery is obtained by subtracting the amount of internally recovered heat from the total amount of latent heat trapped in the vapor. Figure 5d shows the heat recovered from the condensing vapor on each external HX, as well as the heat lost to the environment from each stage (through condensation on the air-/water-cooled HX) (eq S21). External HXs reuse the recovered heat through heating up the incoming feed stream. The bulk heat input ($\dot{Q}_{heat,b}$) is lowered, which increases the GOR. For example, under no-surface-heat conditions, the bulk heat input drops from 2.79×10^4 to 1.87×10^4 W due to external HXs. Based on eq 12, the GOR value increases from 1.45 (without external HXs) to 2.15 (with external HXs). In contrast, the air-/water-cooled HX does not reuse the heat. The heat captured by the air-/water-cooled HX is effectively lost and not accounted for in the GOR calculation (eq 12). When no heat is applied to the membrane surface, the external HXs are able to recover all the heat, up to stage 6, where the available heat exceeds the maximum heat-exchanging capacity of the condensing fluid (3.93×10^3 W for stage 6). However, when 2000 W m^{-2} is applied, the heat in the vapor from stage 4 onward exceeds the capacity of the condensing fluid in the HXs (3.95×10^3, 3.94×10^3, and 3.93×10^3 W for stages 4, 5, and 6). The total amount of heat that is lost in the air-/water-cooled HX increases from 5.02×10^3 W (no-surface-heat input) to 8.42×10^3 W (2000 W m^{-2}). The situation is worsened when 3000 W m^{-2} is applied—in this case, the heat in the vapor exceeds the condensing capacity of the HXs in every stage, except the first stage (3.96×10^3, 3.95×10^3, 3.95×10^3, 3.94×10^3, and 3.93×10^3 W for stages 2, 3, 4, 5, and 6, respectively). The amount of recovered heat that is not reused further increased from 8.42×10^3 W (2000 W m^{-2}) to 1.36×10^4 W (3000 W m^{-2}).

3.3. Comparison between Different Heat Recovery Designs. In a multistage VMD process, the application of additional heat to the membrane surface, when integrated with the external and internal HXs, requires careful consideration to maximize the heat recovery and reuse and the process's GOR. The performance enhancement associated with surface heating is dependent on the design of the heat recovery system in the multistage SHVMD system. Our current design is a hybrid design including both internal HXs and external HXs, whereas the other common heat recovery designs entail only internal HXs (e.g., the commercial V-MEMD process of Memsys)[37] or only external HXs (e.g., numerical simulations from the literature).[18] Therefore, we compare the performance in terms

Downloaded from pubs.acs.org/esthag/article-pdf/57/1/643/2704146/es2c07094.pdf by DOKUZ EYLUL UNIV user on 30 August 2026

https://doi.org/10.1021/acs.est.2c07094
Environ. Sci. Technol. 2023, 57, 643−654

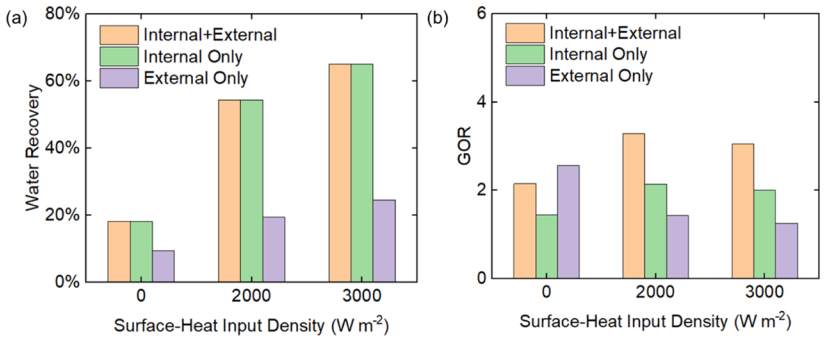

Figure 6. Comparison of (a) water recovery and (b) GOR of a six-stage SHVMD process under different surface heat conditions between the design of hybrid heat recovery, internal heat recovery only, and external heat recovery only.

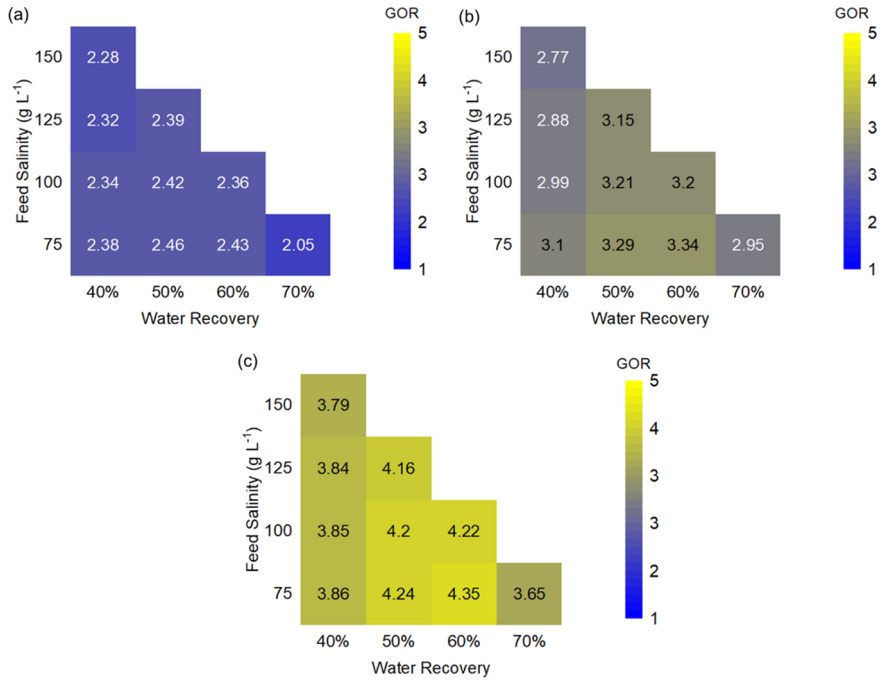

Figure 7. GOR values as a function of feed salinity and water recovery for a (a) four-stage, (b) six-stage, and (c) eight-stage SHVMD process. Under all the conditions shown in the squares at diagonal locations, the TDS concentration of the retentate is 250 g L^{-1} suitable for MLD/ZLD applications. The temperature difference between the influent feed temperature and the distillate-side saturation temperature of the last stage is kept the same to maintain the overall driving force. Water recovery reached the shown values by tuning the surface heat input.

of water recovery and GOR of our current SHVMD design with internal and external HXs to the other two designs employed in standard VMD. Detailed configurations of the two heat recovery designs are provided in Section S5 of the Supporting Information.

In terms of water recovery, the hybrid design is equal to the internal HX-only design, and both designs (18.19, 54.44, and 65.02%) are better than the external HX-only design (9.32, 19.48, and 24.59%), with surface heat densities of 0, 2000, and 3000 W m^{-2}, respectively, all applied to the first stage. In the hybrid design, the internal HXs are responsible for the increase in water recovery with surface heating, whereas the external HXs are not. Water recovery of all three HX configurations increases with the surface heat input (Figure 6a). The internal HXs transfer a portion of the surface-provided heat (added to the first stage only) to all the subsequent stages by capturing and reusing the latent heat of condensation. Therefore, the feed temperature for all subsequent stages is appreciably higher. In contrast, in the external HX-only configuration, the surface-provided heat only increases the feed temperature in the stage to which heat is added (i.e., only in the first stage); the external HXs only add heat to the initial feed stream, which does not mitigate TP or increase water recovery in each stage.

For an SHVMD system, a hybrid HX design achieves higher GOR values where the surface-provided heat is more efficiently captured and reused, compared to the other two designs (Figure 6b). Both the internal HXs and the external HXs contribute to the GOR increase with surface heating in the hybrid design, with the internal HXs having a higher contribution compared to the external HXs. However, if no heat is applied to the membrane surface (i.e., conventional VMD), our model predicts that the highest GOR value is achieved with external HXs (Figure 6b). Recovering and reusing the same amount of heat on external HXs increase GOR more than that on internal HXs. Internal HXs repeatedly heat up the feed in multiple stages, whereas external HXs only heat the feed that is fed to the initial stage to a fixed 90 °C. Therefore, recovering heat on internal HXs leads to more

https://doi.org/10.1021/acs.est.2c07094
Environ. Sci. Technol. 2023, 57, 643−654

Downloaded from pubs.acs.org/esthag/article-pdf/57/1/643/2704146/es2c07094.pdf by DOKUZ EYLUL UNIV user on 30 August 2026

sensible heat in the vapor and retentate that is not reused and a lower GOR. In a hybrid design, the majority of the latent heat in vapor is recovered and reused by internal HXs (2.65×10^4 W), and a relatively small portion of latent heat in vapor is captured and reused by external HXs (9.08×10^3 W). In contrast, in an external HX-only design, all the latent heat in vapor is captured and reused by external HXs (2.08×10^4 W in total). Therefore, due to a higher portion of heat recovered on internal HXs, the hybrid design has a lower GOR value compared to the external HX-only design. Of course, applying no heat to the membrane surface significantly reduces the percentage water recovery (Figure 6a). Hence, the external heat recovery design has a limited potential for brine concentration, which ideally achieves very high water recovery. This comparison of GOR between different heat recovery designs is in agreement with previous studies, which stresses the significance of latent heat recovery in improving the energy efficiency.[54]

3.4. Application toward Hypersaline Brine Concentration. GOR values were evaluated when a multistage SHVMD process was applied toward brine concentration, as GOR values are critical when determining the levelized cost of water.[47] The GOR values of the four-stage, six-stage, and eight-stage SHVMD processes were calculated for feed salinities ranging between 75 and 150 g L^{-1} TDS and for water recovery ranging between 40 and 70% (Figures 7a–c). Detailed information on the four-stage and eight-stage processes is shown in Section S6 of the Supporting Information. In these calculations, the maximum retentate salinity was fixed at 250 g L^{-1}, which is a common target in brine concentration or MLD.

In general, higher GOR values were achieved with a greater number of stages. The number of HXs grows with increasing stages, which enables more heat recovery and higher GOR values. Of course, while increasing the number of stages (and HXs) reduces GOR values, this comes at a cost to the CapEx of the system. Previous techno-economic analyses of the MD process have revealed that the cost of thermal energy (a component of OpEx) is the most significant part of the overall cost of water treatment.[47] Therefore, increasing the number of stages to achieve a higher GOR is an effective strategy to reduce the overall treatment cost.

The relationship between GOR values, water recovery, and feed salinity is not straightforward. GOR values initially increase with a higher water recovery (from 40 to 50%) (Figure 7). However, beyond a certain water recovery threshold, the GOR values decline. Higher water recovery leads to larger masses of vapor that cross the membrane, which has larger amounts of potentially recoverable latent heat. However, both internal and external HXs have a limited capacity of condensing and recovering this heat. After reaching their threshold, any additional heat is not recovered, which reduces the system's GOR. Hence, the optimal region of water recovery is between 50 and 60%. Higher feed salinities negatively impact GOR values, although the impact is not dramatic. Higher salinities reduce the partial vapor pressure of the feed water, which lowers the vapor flux, and leads to a decrease in the mass of vapor that requires condensation. As a result, the overall recovered heat is lower.

4. IMPLICATIONS

Given the enhancement in GOR values and water recovery enabled by surface heating, multistage SHVMD is an attractive approach toward the treatment of high-salinity brine. To compare with other thermal desalination processes, both primary metrics (i.e., water recovery and GOR) and additional metrics (defined in eqs 10, 11, and 13) relevant to CapEx and OpEx of SHVMD and conventional VMD are evaluated (Table 1). In addition, water recovery, GOR, energy efficiency, and specific HX surface area are collected for other thermal desalination technologies (without using any membrane), including mechanical vapor compression (MVC), multistage flash (MSF), and multi-effect distillation (MED), to compare with SHVMD and VMD (Table 1). SHVMD can achieve greater water recovery than that achieved by VMD in this study and similar water recovery to that achieved by other larger-scale VMD and thermal desalination processes. However, SHVMD demonstrates higher GOR and energy efficiency than that of conventional VMD, and both GORs and energy efficiencies are comparable to other large-scale VMD and established thermal desalination technologies.[26,27] It is expected to have higher water recovery, GOR, and energy efficiency when the stage number is further increased (as shown in Section 3.4) and other operating conditions are optimized. We also compared the specific surface area of membranes and HXs between SHVMD and VMD. Both the specific surface areas of SHVMD are lower compared to conventional VMD, which implies that SHVMD may have a lower CapEx. The specific surface areas of the membrane and HX decrease even with a higher surface heat input, which leads to a further lower CapEx. In addition, the specific areas of membranes of both SHVMD and VMD in this study are comparable to the previously reported large-scale VMD processes. In terms of specific areas of HXs, both SHVMD and VMD in this study are less than other large-scale VMD and thermal desalination processes, which show promise of reduced CapEx.

This study was limited to a theoretical system and must be experimentally validated. Before the actual scaling up of the SHVMD process, several aspects that may affect OpEx, CapEx, and system operation need to be considered.

The OpEx of SHVMD is also impacted by the surface heating mechanism, that is, Joule heating or conductive heating. Joule heating is relatively expensive due to the high cost of electricity, leading to a higher OpEx. This approach may be useful when a high amount energy is needed and electrical energy is cheap. In contrast, conductive heating uses cheaper thermal energy, which can lead to a lower OpEx. As both the heat delivery mechanisms rely on metallic or metal-like conductors (e.g., CNTs), the additional CapEx requirements are likely similar.

While our study shows clear advantages in terms of reduced OpEx, a detailed analysis on the CapEx of an SHVMD system must be performed to capture the additional cost of the MD modules, thermal energy carriers, and HXs. In brine concentration, MD is only more cost effective than the state-of-the-art thermal desalination technology, MVC, when the scale of the system is relatively small (<500 m^3 day^{-1}).[17,48] The reason for this is the higher CapEx of MD compared to MVC at a large scale.[48] Therefore, in addition to the total surface area of membranes and HXs, the manufacturing cost per unit surface area of the fixed equipment needs to be considered when the scale is large.

The impact of surface heating on the membrane lifetime (i.e., the stability of membrane materials) is currently unknown. Also, some mineral scalants have reverse solubility, which may increase their scaling potential when the membrane

Downloaded from pubs.acs.org/esthag/article-pdf/57/1/643/2704146/es2c07094.pdf by DOKUZ EYLUL UNIV user on 30 August 2026

https://doi.org/10.1021/acs.est.2c07094
Environ. Sci. Technol. 2023, 57, 643–654

Table 1. Comparison of the Cost-Relevant Parameters between Six-stage SHVMD and Six-stage Conventional VMD with both Internal and External HXs and other Large-Scale VMD, MVC, MSF, and MED[a]

configuration	SHVMD (2000 W m^{-2}, this study)	SHVMD (3000 W m^{-2}, this study)	VMD (this study)	VMD (previous studies)	MVC	MSF	MED
water recovery	54.44% (100 g L^{-1} TDS feed)	65.02% (100 g L^{-1} TDS feed)	18.19% (100 g L^{-1} TDS feed)	13–65% (0.02–35 gL^{-1} TDS feed)[37]	40% (38 gL^{-1} TDS feed)[55]	<80% (35 gL^{-1} TDS feed)[56]	20–42% (35–42 g L^{-1} TDS)[57]
GOR	3.28	3.06	2.15	1.52–3.4,[37] 0.5–0.8,[21] 2.8–7[18]	16–22[58]	1.1–16[17]	1.1–14[17]
energy efficiency	3.10%	3.02%	1.93%	1.28–2.9%,[37] 0.4–0.68%,[21] 2.4–6.0%[18]	7–15%[59]	5–15%[59]	2–20%[59]
membrane surface area per liter of distillate (m^2 s L^{-1})	225.66	189.09	677.38	190.1–1088.6,[18] 134.09–231.15[60]			
HX surface area per liter of distillate (m^2 s L^{-1})	34.59	28.47	82.27	150.94–260.19[60]	42–160[61]	270–600[62]	350–1600[63]

[a]Different surface heat input densities are presented with SHVMD configuration.

surface is heated and reduce the membrane's life span.[64] Nevertheless, in a previous lab-scale DHVMD study where we concentrated real produced water, we observed stable membrane operations and did not observe noticeable scaling until 50% recovery was achieved, with a dramatic reduction in flux only after 60% recovery.[10] In addition, in Joule heating MD, the oxidation of the CNT layer of the membrane was minimized by using alternating currents instead of direct currents.[39] The elevated surface temperature might induce faster crystallization of $CaSO_4$, a common scaling species, on the membrane surface. This side effect can be mitigated by limiting the total heat input to an extent just reducing the TP instead of having a high surface temperature compared to the bulk feed temperature. Furthermore, multiple antiscaling strategies exist that can be leveraged to minimize mineral scaling in MD.[65] Therefore, mineral scaling is not likely to dramatically impact our model results but is certainly worth investigating in future studies.

■ ASSOCIATED CONTENT

Supporting Information

The Supporting Information is available free of charge at https://pubs.acs.org/doi/10.1021/acs.est.2c07094.

Additional modeling details including the assumptions and parameters of the model; specific governing equations for heat and mass transfer; supporting process performance metrics; performance comparison with different ways of adding heating; alternative designs of heat recovery; and parameters for brine concentration case studies (PDF)

■ AUTHOR INFORMATION

Corresponding Author

David Jassby − *Department of Civil and Environmental Engineering, University of California Los Angeles, Los Angeles, California 90095, United States; California NanoSystems Institute and Institute of the Environment & Sustainability, University of California Los Angeles, Los Angeles, California 90095, United States;* orcid.org/0000-0002-2133-2536; Phone: (310) 825-1346; Email: jassby@ucla.edu

Authors

Yiming Liu − *Department of Civil and Environmental Engineering, University of California Los Angeles, Los Angeles, California 90095, United States;* orcid.org/0000-0003-4761-5531

Jingbo Wang − *Department of Civil and Environmental Engineering, University of California Los Angeles, Los Angeles, California 90095, United States*

Eric M.V. Hoek − *Department of Civil and Environmental Engineering, University of California Los Angeles, Los Angeles, California 90095, United States; California NanoSystems Institute and Institute of the Environment & Sustainability, University of California Los Angeles, Los Angeles, California 90095, United States; Energy Technologies Area, Lawrence Berkeley National Laboratory, Berkeley, California 94720, United States;* orcid.org/0000-0002-5748-6481

Federico Municchi − *Department of Mechanical Engineering, Colorado School of Mines, Golden, Colorado 80401, United States*

https://doi.org/10.1021/acs.est.2c07094
Environ. Sci. Technol. 2023, 57, 643−654

Downloaded from pubs.acs.org/esthag/article-pdf/57/1/643/2704146/es2c07094.pdf by DOKUZ EYLUL UNIV user on 30 August 2026

Nils Tilton − *Department of Mechanical Engineering, Colorado School of Mines, Golden, Colorado 80401, United States*

Tzahi Y. Cath − *Department of Civil and Environmental Engineering, Colorado School of Mines, Golden, Colorado 80401, United States;* orcid.org/0000-0002-0669-4117

Craig S. Turchi − *Thermal Energy Science & Technologies Research Group, National Renewable Energy Laboratory, Golden, Colorado 80401, United States*

Michael B. Heeley − *Department of Economics and Business, Colorado School of Mines, Golden, Colorado 80401, United States*

Complete contact information is available at: https://pubs.acs.org/10.1021/acs.est.2c07094

Notes

The authors declare no competing financial interest.

■ ACKNOWLEDGMENTS

This work was supported by the Department of Energy (DOE) (award no. DE-EE0008391), the UCLA Samueli School of Engineering, the UCLA Department of Civil & Environmental Engineering, and the UCLA Sustainable LA Grand Challenge (EMVH). The authors thank all the colleagues in the Jassby group for their support and Mr. Erfan Sedighi and Dr. Y. Sungtaek Ju from the Department of Mechanical and Aerospace Engineering at UCLA for their helpful suggestions.

■ REFERENCES

(1) Whittemore, D. O. Geochemical differentiation of oil and gas brine from other saltwater sources contaminating water resources: Case studies from Kansas and Oklahoma. *Environ. Geosci.* **1995**, *2*, 15−31.

(2) Pramanik, B. K.; Nghiem, L. D.; Hai, F. I. Extraction of strategically important elements from brines: Constraints and opportunities. *Water Res.* **2020**, *168*, 115149.

(3) Panagopoulos, A.; Haralambous, K. J.; Loizidou, M. Desalination brine disposal methods and treatment technologies—A review. *Sci. Total Environ.* **2019**, *693*, 133545.

(4) McFeeters, R. F.; Pérez-Díaz, I. Fermentation of cucumbers brined with calcium chloride instead of sodium chloride. *J. Food Sci.* **2010**, *75*, C291−C296.

(5) Hoek, E. M.; Jassby, D.; Kaner, R. B.; Wu, J.; Wang, J.; Liu, Y.; Rao, U.*Sustainable Desalination and Water Reuse*; Synthesis Lectures on Sustainable Development; Springer, 2021; Vol. 2; pp 1−204.

(6) Bruinsma, O.; Branken, D.; Lemmer, T.; van der Westhuizen, L.; Rossouw, S. Sodium sulfate splitting as zero brine process in a base metal refinery: Screening and optimization in batch mode. *Desalination* **2021**, *511*, 115096.

(7) Ahmad, N.; Baddour, R. E. A review of sources, effects, disposal methods, and regulations of brine into marine environments. *Ocean Coast. Manag.* **2014**, *87*, 1−7.

(8) Tang, X.; Kum, S.; Liu, H. Inland desalination brine disposal: A baseline study from southern California on brine transport infrastructure and treatment potential. *ACS ES&T Engg* **2021**, *2*, 456−464.

(9) Davenport, D. M.; Deshmukh, A.; Werber, J. R.; Elimelech, M. High-Pressure Reverse Osmosis for Energy-Efficient Hypersaline Brine Desalination: Current Status, Design Considerations, and Research Needs. *Environ. Sci. Technol. Lett.* **2018**, *5*, 467−475.

(10) Liu, Y.; Wang, J.; Jung, B.; Rao, U.; Sedighi, E.; Hoek, E. M. V.; Tilton, N.; Cath, T. Y.; Turchi, C. S.; Heeley, M. B.; Ju, Y. S.; Jassby, D. Desalinating a real hyper-saline pre-treated produced water via direct-heat vacuum membrane distillation. *Water Res.* **2022**, *218*, 118503.

(11) Wang, Z.; Feng, D.; Chen, Y.; He, D.; Elimelech, M. Comparison of Energy Consumption of Osmotically Assisted Reverse Osmosis and Low-Salt-Rejection Reverse Osmosis for Brine Management. *Environ. Sci. Technol.* **2021**, *55*, 10714−10723.

(12) Cipolletta, G.; Lancioni, N.; Akyol, C.; Eusebi, A. L.; Fatone, F. Brine treatment technologies towards minimum/zero liquid discharge and resource recovery: State of the art and techno-economic assessment. *J. Environ. Manage.* **2021**, *300*, 113681.

(13) Boo, C.; Billinge, I. H.; Chen, X.; Shah, K. M.; Yip, N. Y. Zero liquid discharge of ultrahigh-salinity brines with temperature swing solvent extraction. *Environ. Sci. Technol.* **2020**, *54*, 9124−9131.

(14) Shaulsky, E.; Wang, Z. X.; Deshmukh, A.; Karanikola, V.; Elimelech, M. Membrane distillation assisted by heat pump for improved desalination energy efficiency. *Desalination* **2020**, *496*, 114694.

(15) Alrehaili, O.; Perreault, F.; Sinha, S.; Westerhoff, P. Increasing net water recovery of reverse osmosis with membrane distillation using natural thermal differentials between brine and co-located water sources: Impacts at large reclamation facilities. *Water Res.* **2020**, *184*, 116134.

(16) Shah, K. M.; Billinge, I. H.; Chen, X.; Fan, H.; Huang, Y.; Winton, R. K.; Yip, N. Y. Drivers, challenges, and emerging technologies for desalination of high-salinity brines: A critical review. *Desalination* **2022**, *538*, 115827.

(17) Deshmukh, A.; Boo, C.; Karanikola, V.; Lin, S. H.; Straub, A. P.; Tong, T. Z.; Warsinger, D. M.; Elimelech, M. Membrane distillation at the water-energy nexus: limits, opportunities, and challenges. *Energy Environ. Sci.* **2018**, *11*, 1177−1196.

(18) Chung, H. W.; Swaminathan, J.; Warsinger, D. M.; Lienhard V, J. H. Multistage vacuum membrane distillation (MSVMD) systems for high salinity applications. *J. Membr. Sci.* **2016**, *497*, 128−141.

(19) Said, I. A.; Wang, S.; Li, Q. L. Field Demonstration of a Nanophotonics-Enabled Solar Membrane Distillation Reactor for Desalination. *Ind. Eng. Chem. Res.* **2019**, *58*, 18829−18835.

(20) Lin, S. H.; Yip, N. Y.; Elimelech, M. Direct contact membrane distillation with heat recovery: Thermodynamic insights from module scale modeling. *J. Membr. Sci.* **2014**, *453*, 498−515.

(21) Summers, E. K.; Arafat, H. A.; Lienhard, J. H. Energy efficiency comparison of single-stage membrane distillation (MD) desalination cycles in different configurations. *Desalination* **2012**, *290*, 54−66.

(22) Bartholomew, T. V.; Dudchenko, A. V.; Siefert, N. S.; Mauter, M. S. Cost optimization of high recovery single stage gap membrane distillation. *J. Membr. Sci.* **2020**, *611*, 118370.

(23) Swaminathan, J.; Lienhard, J. H. Design and operation of membrane distillation with feed recirculation for high recovery brine concentration. *Desalination* **2018**, *445*, 51−62.

(24) Gilron, J.; Song, L.; Sirkar, K. K. Design for cascade of crossflow direct contact membrane distillation. *Ind. Eng. Chem. Res.* **2007**, *46*, 2324−2334.

(25) Dudchenko, A. V.; Bartholomew, T. V.; Mauter, M. S. Cost optimization of multi-stage gap membrane distillation. *J. Membr. Sci.* **2021**, *627*, 119228.

(26) Brogioli, D.; La Mantia, F. Electrochemical Methods for Exploiting Low-Temperature Heat Sources: Challenges in Material Research. *Adv. Energy Mater.* **2022**, *12*, 2103842.

(27) Brogioli, D.; La Mantia, F. Innovative technologies for energy production from low temperature heat sources: critical literature review and thermodynamic analysis. *Energy Environ. Sci.* **2021**, *14*, 1057−1082.

(28) Nayar, K. G.; Sharqawy, M. H.; Lienhard, J.*Seawater Thermophysical Properties Library*, 2016.

(29) Eykens, L.; Reyns, T.; De Sitter, K.; Dotremont, C.; Pinoy, L.; Van der Bruggen, B. How to select a membrane distillation configuration? Process conditions and membrane influence unraveled. *Desalination* **2016**, *399*, 105−115.

(30) Karanikola, V.; Moore, S. E.; Deshmukh, A.; Arnold, R. G.; Elimelech, M.; Sáez, A. E. Economic performance of membrane distillation configurations in optimal solar thermal desalination systems. *Desalination* **2019**, *472*, 114164.

(31) Wang, J. B.; Liu, Y. M.; Rao, U.; Dudley, M.; Ebrahimi, N. D.; Lou, J. C.; Han, F.; Hoek, E. M. V.; Tilton, N.; Cath, T. Y.; Turchi, C.

Downloaded from pubs.acs.org/esthag/article-pdf/57/1/643/2704146/es2c07094.pdf by DOKUZ EYLUL UNIV user on 30 August 2026

S.; Heeley, M. B.; Ju, Y. S.; Jassby, D. Conducting thermal energy to the membrane/water interface for the enhanced desalination of hypersaline brines using membrane distillation. *J. Membr. Sci.* **2021**, *626*, 119188.
(32) Boutikos, P.; Mohamed, E. S.; Mathioulakis, E.; Belessiotis, V. A theoretical approach of a vacuum multi-effect membrane distillation system. *Desalination* **2017**, *422*, 25−41.
(33) Kim, Y.-D.; Thu, K.; Choi, S. H. Solar-assisted multi-stage vacuum membrane distillation system with heat recovery unit. *Desalination* **2015**, *367*, 161−171.
(34) Kiefer, F.; Spinnler, M.; Sattelmayer, T. Multi-Effect Vacuum Membrane Distillation systems: Model derivation and calibration. *Desalination* **2018**, *438*, 97−111.
(35) Omar, A.; Li, Q. Y.; Nashed, A.; Guan, J.; Dai, P.; Taylor, R. A. Experimental and numerical investigation of a new hollow fiber-based multi-effect vacuum membrane distillation design. *Desalination* **2021**, *501*, 114908.
(36) Andrés-Mañas, J. A.; Ruiz-Aguirre, A.; Acién, F.; Zaragoza, G. Assessment of a pilot system for seawater desalination based on vacuum multi-effect membrane distillation with enhanced heat recovery. *Desalination* **2018**, *443*, 110−121.
(37) Zhao, K.; Heinzl, W.; Wenzel, M.; Büttner, S.; Bollen, F.; Lange, G.; Heinzl, S.; Sarda, N. Experimental study of the memsys vacuum-multi-effect-membrane-distillation (V-MEMD) module. *Desalination* **2013**, *323*, 150−160.
(38) Burhan, M.; Shahzad, M. W.; Ybyraiymkul, D.; Oh, S. J.; Ghaffour, N.; Ng, K. C. Performance investigation of MEMSYS vacuum membrane distillation system in single effect and multi-effect mode. *Sustain. Energy Technol. Assess.* **2019**, *34*, 9−15.
(39) Dudchenko, A. V.; Chen, C.; Cardenas, A.; Rolf, J.; Jassby, D. Frequency-dependent stability of CNT Joule heaters in ionizable media and desalination processes. *Nat. Nanotechnol.* **2017**, *12*, 557−563.
(40) Mustakeem, M.; Qamar, A.; Alpatova, A.; Ghaffour, N. Dead-end membrane distillation with localized interfacial heating for sustainable and energy-efficient desalination. *Water Res.* **2021**, *189*, 116584.
(41) Zuo, K.; Wang, W.; Deshmukh, A.; Jia, S.; Guo, H.; Xin, R.; Elimelech, M.; Ajayan, P. M.; Lou, J.; Li, Q. Multifunctional nanocoated membranes for high-rate electrothermal desalination of hypersaline waters. *Nat. Nanotechnol.* **2020**, *15*, 1025−1032.
(42) Huang, J.; He, Y. R.; Shen, Z. H. Joule heating membrane distillation enhancement with multi-level thermal concentration and heat recovery. *Energy Convers. Manage.* **2021**, *238*, 114111.
(43) Li, K.; Zhang, Y.; Wang, Z.; Liu, L.; Liu, H.; Wang, J. Electrothermally Driven Membrane Distillation for Low-Energy Consumption and Wetting Mitigation. *Environ. Sci. Technol.* **2019**, *53*, 13506−13513.
(44) Han, F.; Bian, Y.; Zhang, C. Conductive heating vacuum membrane distillation for brine desalination: Study on operational conditions, temperature polarization and energy consumption. *Desalination* **2022**, *531*, 115726.
(45) Anvari, A.; Azimi Yancheshme, A. A.; Kekre, K. M.; Ronen, A. State-of-the-art methods for overcoming temperature polarization in membrane distillation process: A review. *J. Membr. Sci.* **2020**, *616*, 118413.
(46) Chen, X.; Yip, N. Y. Unlocking high-salinity desalination with cascading osmotically mediated reverse osmosis: Energy and operating pressure analysis. *Environ. Sci. Technol.* **2018**, *52*, 2242−2250.
(47) Tavakkoli, S.; Lokare, O. R.; Vidic, R. D.; Khanna, V. A techno-economic assessment of membrane distillation for treatment of Marcellus shale produced water. *Desalination* **2017**, *416*, 24−34.
(48) Schwantes, R.; Chavan, K.; Winter, D.; Felsmann, C.; Pfafferott, J. Techno-economic comparison of membrane distillation and MVC in a zero liquid discharge application. *Desalination* **2018**, *428*, 50−68.
(49) Alsaadi, A. S.; Ghaffour, N.; Li, J. D.; Gray, S.; Francis, L.; Maab, H.; Amy, G. L. Modeling of air-gap membrane distillation process: A theoretical and experimental study. *J. Membr. Sci.* **2013**, *445*, 53−65.
(50) Andrés-Mañas, J. A.; Requena, I.; Zaragoza, G. Characterization of the use of vacuum enhancement in commercial pilot-scale air gap membrane distillation modules with different designs. *Desalination* **2022**, *528*, 115490.
(51) Zaragoza, G.; Andres-Manas, J. A.; Ruiz-Aguirre, A. Commercial scale membrane distillation for solar desalination. *npj Clean Water* **2018**, *1*, 20.
(52) Kharraz, J. A.; Farid, M. U.; von Eiff, D.; Gao, Y.; Shi, Z.; An, A. K.Hybrid configuration of membrane distillation: vacuum multi-effect membrane distillation. *Membrane Distillation: Materials and Processes*; Nova Science Publishers, Inc., 2020.
(53) Christie, K. S. S.; Horseman, T.; Lin, S. H. Energy efficiency of membrane distillation: Simplified analysis, heat recovery, and the use of waste-heat. *Environ. Int.* **2020**, *138*, 105588.
(54) Patel, S. K.; Ritt, C. L.; Deshmukh, A.; Wang, Z. X.; Qin, M. H.; Epsztein, R.; Elimelech, M. The relative insignificance of advanced materials in enhancing the energy efficiency of desalination technologies. *Energy Environ. Sci.* **2020**, *13*, 1694−1710.
(55) Shaffer, D. L.; Arias Chavez, L. H.; Ben-Sasson, M.; Romero-Vargas Castrillón, S.; Yip, N. Y.; Elimelech, M. Desalination and reuse of high-salinity shale gas produced water: drivers, technologies, and future directions. *Environ. Sci. Technol.* **2013**, *47*, 9569−9583.
(56) Turek, M. Seawater desalination and salt production in a hybrid membrane-thermal process. *Desalination* **2003**, *153*, 173−177.
(57) Filippini, G.; Al-Obaidi, M.; Manenti, F.; Mujtaba, I. M. Performance analysis of hybrid system of multi effect distillation and reverse osmosis for seawater desalination via modelling and simulation. *Desalination* **2018**, *448*, 21−35.
(58) Tong, T.; Carlson, K. H.; Robbins, C. A.; Zhang, Z.; Du, X. Membrane-based treatment of shale oil and gas wastewater: The current state of knowledge. *Front. Environ. Sci. Eng.* **2019**, *13*, 63.
(59) Lin, S. Energy efficiency of desalination: fundamental insights from intuitive interpretation. *Environ. Sci. Technol.* **2019**, *54*, 76−84.
(60) Lee, J.-G.; Kim, W.-S. Numerical study on multi-stage vacuum membrane distillation with economic evaluation. *Desalination* **2014**, *339*, 54−67.
(61) Alasfour, F. N.; Abdulrahim, H. K. The effect of stage temperature drop on MVC thermal performance. *Desalination* **2011**, *265*, 213−221.
(62) Junjie, Y.; Shufeng, S.; Jinhua, W.; Jiping, L. Improvement of a multi-stage flash seawater desalination system for cogeneration power plants. *Desalination* **2007**, *217*, 191−202.
(63) Al-Mutaz, I. S.; Wazeer, I. Comparative performance evaluation of conventional multi-effect evaporation desalination processes. *Appl. Therm. Eng.* **2014**, *73*, 1194−1203.
(64) Horseman, T.; Yin, Y.; Christie, K. S.; Wang, Z.; Tong, T.; Lin, S. Wetting, scaling, and fouling in membrane distillation: state-of-the-art insights on fundamental mechanisms and mitigation strategies. *ACS ES&T Engg* **2020**, *1*, 117−140.
(65) Hickenbottom, K. L.; Cath, T. Y. Sustainable operation of membrane distillation for enhancement of mineral recovery from hypersaline solutions. *J. Membr. Sci.* **2014**, *454*, 426−435.

Downloaded from pubs.acs.org/esthag/article-pdf/57/1/643/2704146/es2c07094.pdf by DOKUZ EYLUL UNIV user on 30 August 2026

https://doi.org/10.1021/acs.est.2c07094
Environ. Sci. Technol. 2023, 57, 643−654